Thin Solid Films 670 (2019) 6–16

Contents lists available at ScienceDirect

Thin Solid Films

journal homepage: www.elsevier.com/locate/tsf

Effect of defects and secondary phases in Cu_2ZnSnS_4 absorber material on the performance of Zn(O,S) buffered devices

Fulya Turkoglu[a,*], Hasan Koseoglu[a], Ayten Cantas[a,c], Fatime G. Akca[a], Ece Meric[a], Dilara G. Buldu[a], Mehtap Ozdemir[b], Enver Tarhan[a], Lutfi Ozyuzer[a,b], Gulnur Aygun[a]

[a] Department of Physics, Izmir Institute of Technology, 35430 Urla, Izmir, Turkey
[b] Teknoma Technological Materials Ltd., IZTEKGEB, IYTE Campus, Urla, Izmir, Turkey
[c] Department of Electric and Energy, Pamukkale University, Kınıklı 20160, Denizli, Turkey

ARTICLE INFO

Keywords:
Copper zinc tin sulfide
Zinc oxysulfide
Absorber layer
Buffer layer
Magnetron sputtering

ABSTRACT

Copper zinc tin sulfide (CZTS) absorber layer attracts so much attention in photovoltaic industry since it contains earth abundant, low cost and non-toxic elements contrary to other chalcogenide based solar cells. In the present work, CZTS absorber layers were prepared following a two-stage process: firstly, a stack of metal precursors (Copper (Cu)/Tin (Sn)/Zinc (Zn)/Copper (Cu)) were deposited on molybdenum (Mo) substrate by magnetron sputtering, then this stack was annealed under S atmosphere inside a tubular furnace. CZTS thin films were investigated using energy dispersive X-ray spectroscopy, X-ray diffraction, scanning electron microscopy and Raman spectroscopy. The effect of sulfurization time and the thickness of top and bottom Cu layer in precursors on the properties of CZTS thin films were investigated. The importance of Cu thickness adjacent to Sn to avoid detrimental phases was addressed. The significance of sulfurization time to restrict the Sn and Zn losses, formation of oxides such as tin dioxide and zinc oxide, and formation of molybdenum disulfide and voids between Mo/CZTS interface was also addressed. Moreover, cadmium sulfide buffer layer, which is conventionally used in CZTS solar cells, is replaced by an environmentally friendly alternative zinc oxysulfide buffer layer.

1. Introduction

Currently, there exist two major thin film technologies that have been commercialized, namely cadmium telluride (CdTe) and copper indium gallium diselenide ($CuIn_xGa_{1-x}(S,Se)_2$, or CIGS). These technologies have high conversion efficiencies both in commercial production and in laboratory scale. Conversion efficiencies have reached recently up to 22.1% [1] for CdTe and 22.6% [2] for CIGS. Despite the higher conversion efficiencies of these semiconductors, the toxicity of cadmium (Cd) element and, availability problem and high cost of indium and Gallium elements restrict the production capacity of these thin film solar cells. Non-toxic and earth abundant materials are needed for long term viability of thin film solar cells. One such material is copper zinc tin sulfide (Cu_2ZnSnS_4); commonly known as CZTS. Since this material is non-toxic and its component elements are abundant in the earth's crust, CZTS solar cells are free from both resource-saving concerns and environmental pollution. In addition, CZTS is a p-type semiconductor with talented physical properties, such as the direct band gap of 1.5 eV, high optical absorption coefficient ($> 10^{-4}\,cm^{-1}$), low thermal conductivity, etc. [3,4]. Band gap of CZTS is ideal to convert the maximum amount of energy from the solar spectrum into electricity [5]. Owing to its high absorption coefficient, only a few microns thick layer of CZTS is enough to absorb all the photons with energies above its band gap. Due to these important features, CZTS is expected to be one of the promising materials for thin film solar cells. To date, the world record efficiencies of 9.2% and 9.4% for pure sulfide CZTS solar cell have been achieved by Hiroi, et al. and Tajima, et al., respectively [6,7]. Although this is somewhat less efficient than the current efficiencies of other technologies, it offers a cost-effective solution by utilizing less expensive materials and large-scale production [8].

There are several reasons for the poorer photoconversion efficiencies of CZTS based solar cells. Control of secondary phase formation in CZTS is a main point for achieving high efficiency devices. Binary and ternary secondary phases such as copper (II) sulfide (CuS), copper (I) sulfide (Cu_2S), copper tin sulfide (Cu_2SnS_3), zinc sulfide (ZnS), tin sulfide (SnS), and tin disulfide (SnS_2) can easily form during the growth process of CZTS since single phase CZTS can be formed in a very narrow stability region in phase diagram [9,10]. Moreover, CZTS shows low thermal stability at high temperature ($> 500\,^{\circ}C$) [11]. CZTS

* Corresponding author.
E-mail address: fulyaturkoglu@iyte.edu.tr (F. Turkoglu).

https://doi.org/10.1016/j.tsf.2018.12.001
Received 24 March 2018; Received in revised form 8 November 2018; Accepted 2 December 2018
Available online 04 December 2018
0040-6090/

decomposes into solid Cu_2S and ZnS due to the evaporation of SnS and sulfur (S) from the film at high temperatures [12]. Because of the formation of tin (Sn)-depleted surfaces, Sn vacancies, and Cu_2S and ZnS secondary phases, the performance of CZTS solar cells degrades. Therefore, it is extremely important to reduce Sn loss during annealing to achieve highly efficient CZTS devices. Intrinsic defects in CZTS absorber layer also play an important role in view of solar cell performances. Several intrinsic point defects are possible for CZTS quaternary compound, including antisite defects (Cu_{Zn}, Zn_{Cu}, Cu_{Sn}, Sn_{Cu}, Zn_{Sn}, and Sn_{Zn}), vacancies (V_{Cu}, V_{Zn}, V_{Sn}, and V_S) and interstitial defects (Cu_i, Zn_i, and Sn_i) [13]. These defects can manifest as shallow or deep levels within the band gap, can serve as donor or acceptor, and can act as traps or recombination centers, thus the opto-electronic properties of the host material are affected. It has been shown that CZTS absorber layer with copper (Cu)-poor and zinc (Zn)-rich composition are generally accepted in the literature for the realization of high efficiency CZTS devices [14,15] since this composition suppress the formation of deep level defects like Cu_{Sn} and harmful secondary phases like CuS and Cu_2S. The Cu-poor and Zn-rich composition of CZTS films with Cu/(Zn + Sn) ≈ 0.8 and Zn/Sn ≈ 1.2 is suggested as the most suitable composition for high-performance solar cells both theoretically [16] and experimentally [17–20].

Stacking order of the precursor also plays an important role on the performance of the CZTS solar cells since it affects the chemical composition, morphology and phase of the resulting CZTS thin film [21]. Araki et al. prepared CZTS films by the sulfurization of electron-beam-evaporated metal precursors with six different stacking orders to create three-layered films [22]. It was reported that higher conversion efficiency (η) can be obtained when Cu and Sn adjacent to each other in the precursor film. Different stack sequences Cu, Zn and Sn were deposited on Mo-coated glass by sputtering [23]. Voids were observed for all CZTS films, especially for CZTS films fabricated using precursor that Cu is not adjacent to Sn. Based on the results in [22], they concluded that when Cu is not adjacent to Sn, it's difficult to form Cu_2SnS_3 which is reactant to produce CZTS with ZnS. Stack sequences of Mo/Zn/Cu/Sn and Mo/Zn/Sn/Cu were fabricated by Fernandes et al. and they reported that the Cu layer on top reduces the loss of Zn and Sn and allows CZTS films with better crystal quality [24]. Detailed growth path of CZTS was reported by Su et al. [25]. It was found that CZTS with high phase purity can be obtained by controlling the stacking order and the Cu/(Sn + Zn) ratio. A phase purity as high as 93% was obtained by having Cu and Sn adjacent to each other in the precursors. They showed that the existence of and reaction among Cu_2S, Cu_2SnS_3 and ZnS, which depend on the stacking order, determine the percentage of CZTS. When more Cu_2SnS_3 was formed, more CZTS was obtained. By considering the last stage reaction to form CZTS, it was realized that most complete sulfurization and higher percentage of CZTS can be obtained by reduced percentages of both cubic Cu_2SnS_3 and ZnS in the final film. Moreover, when both Cu_2SnS_3 and ZnS do not decrease simultaneously, the sulfurization is less complete and therefore the final reaction is inhibited such that the CZTS phase is the lowest.

Currently the standard technique of producing CZTS solar cells is to use cadmium sulfide (CdS) grown by chemical bath deposition (CBD) as buffer layer. Although yielding the best device performance, there are some debates on the fundamental issues with this buffer layer. Firstly, it contains toxic Cd. Secondly, the CBD process implies additional production costs compared to the dry process when industrially implemented. In addition, the usage of a material with a wider bandgap (E_g) than CdS ($E_{g(CdS)}$ = 2.4 eV) [26] could lead to increase in the cell performance due to minimization of the photon loss in the blue wavelength range. Therefore, alternative materials are being sought that can replace this layer with something that is environmentally suitable and that does not lower the performance. Among the different alternatives to CdS, zinc oxysulfide (Zn(O,S)) alloys has emerged to be one of the most promising candidates for this purpose. The S/(S + O) ratio in Zn(O,S) can be easily varied by changing the experimental parameters, for example, changing O_2/Ar gas mixture ratio during sputtering. As their composition is varied, key parameters such as conduction band offset (CBO), E_g, and conductivity can be precisely tuned [27–31]. A large E_g (2.6–3.8 eV) of Zn(O,S) allows a greater collection of high-energy electrons, and thus reducing the photocurrent loss in the short wavelength region. Moreover, recombination at the buffer interface can be minimized by the careful adjustment of the S content [32]. Furthermore, variations of the S and O contents in the Zn(O,S) buffer layer allows the tuning of the CBO value at the p-n junction interface, giving extra possibility to increase the efficiency.

The highest reported efficiencies for CIGS solar cells have been achieved by the Zn(O,S) buffer layers deposited either by CBD or Atomic Layer Deposition (ALD), 20.9% [33] and 21.0% [34], respectively. Recently, CIGSe devices with efficiencies exceeding 18% were also obtained by using a Zn(O,S) buffer layer grown by RF-sputtering from a mixed target with an argon (Ar) pressure of 0.5 Pa [35]. So far, very few experimental attempts have been made to investigate the performance of CZTS/Zn(O,S) devices (pure sulfide). Ericson et al. evaluated S to O ratios of Zn(O,S) films grown by ALD to find an appropriate CBO between the CZTS absorber and the Zn(O,S) buffer [36]. The best CZTS/Zn(O,S) device with an efficiency of 4.6% was achieved by Zn(O,S) 6:1 buffer, and the best reference cell with CdS buffer gave 7.3% efficiency. Yan et al. investigated band alignment between CZTS absorber and Zn(O,S) buffer. However, no efficiency was measured for the device with a Zn(O,S) buffer due to the high CBO of around 0.9 eV [37].

In the present work, fabrication of CZTS thin films was performed by a two-stage process: firstly, a stack of metal precursors was deposited by magnetron sputtering, then this stack was annealed under S atmosphere. These precursors have the same stacking order (Cu/Sn/Zn/Cu) but have different thicknesses of Cu shared between top and bottom of the precursor stack. These precursor stacks sulfurized for different durations which is one of the most important parameter for the formation of the CZTS absorber material with desired stoichiometry and optimal crystalline quality. The effect of sulfurization time and the thickness of top and bottom Cu layer in precursors on the properties of CZTS thin films were investigated. The importance of thickness of Cu layer adjacent to Sn and sulfurization time to avoid detrimental phases, to restrict the Sn and Zn losses and to get higher quality CZTS absorber layers were addressed. The performance of these absorbers in CZTS solar cells fabricated by environmentally friendly Zn(O,S) buffer layer were further investigated. All thin films used to form CZTS solar cell structure were deposited entirely using only the magnetron sputtering technique since sputtering offers a wide range of advantages, such as high adhesion of films, excellent coverage, easy adaptation to large-scale and reproducible manufacturing. Moreover, in the literature, CZTS solar cell with the highest efficiency has been grown by a sputtering technique [7].

2. Experimental

Mo electrode layers with the thickness around 1 μm were deposited on soda-lime glass (SLG) substrates by DC magnetron sputtering. Bi-layer deposition process was used to ensure good adhesion to SLG and good electrical properties for Mo layers [38,39]. The deposition of Mo was started at a higher working pressure (1.67 Pa) and then decreased to lower working pressure (0.33 Pa) (Teknoma Technological Materials Industrial and Trading Inc.). Fabrication of CZTS thin films was performed by a two-stage process. In the first stage of the process, Cu, Zn, and Sn metallic precursors were deposited sequentially on Mo coated SLG substrates by multi target DC magnetron sputtering from 2-in.-targets of Cu (99.999%), Zn (99.99%) and Sn (99.999%) at room temperature [4,40]. The Mo coated SLGs were loaded in the system and the chamber was evacuated to a base pressure of 1.07 mPa. Pure Ar gas with 30 standard cubic centimeters per minute (sccm) flowing rate was fed into the chamber and the working pressure was maintained at

0.66 Pa during the sputtering. In order to grow sequentially layered metallic precursors in the Cu/Sn/Zn/Cu layer ordering, 41, 40, 20 and 41 W DC bias was applied to the Cu, Zn, Sn and Cu targets, respectively. Sputtering power and deposition time were adjusted to obtain a 630 nm thick precursor to have Cu, Sn and Zn layers with the thickness of 175, 165 and 290 nm, respectively. These metal ratios were chosen by considering the stoichiometry reported in the literature for most efficient CZTS based solar cells which have Zn-rich and Cu-poor nominal composition, close to Cu:Zn:Sn:S = 1.80:1.20:1.00:4 [14, 15, 17, 41]. Using the same stacking order, two types of precursors having different thicknesses of Cu. The structure of Type 1 is SLG/Mo/Cu(55 nm)/Sn (290 nm)/Zn(165 nm)/Cu(120 nm) and Type2 is SLG/Mo/Cu(120 nm)/Sn(290 nm)/Zn(165 nm)/Cu(55 nm) were fabricated. For both Type 1 and Type 2 structures, Cu layer deposited on the top of the stack since Cu is non-volatile (low vapor pressure at 2.3 μPa) and it protects the loss of volatile Sn and Zn. Therefore, capping with Cu minimize Sn loss during the sulfurization process and prevent the ZnS formation over the surface CZTS. Moreover, Cu layer at the bottom of the precursor stack prevent the adhesion problem of the Zn and Sn to the Mo surface according to our preliminary works. Sulfurization of the metallic precursor to synthesize CZTS absorber layer was performed in a Lindberg/Blue M tube furnace under Ar atmosphere. The precursor stack was positioned on the middle of the quartz tube on a graphite support which has a good thermal conductivity and was used to provide a low temperature gradient throughout the thickness of the sample. 600 mg S powder (Scharlau, synthesis grade, 99% purity) in a graphite box was weighted and placed 18 cm away from the precursor stack into the quartz tube. 70 sccm Ar was flowed into the quartz tube by a MKS 647C mass flow controller as a carrier gas during the sulfurization process. The pressure of the quartz tube was maintained at atmospheric level. Specific temperature profile was fallowed during sulfurization: ramp of 10 K per minutes is used and firstly stopped at 543.15 K for three minutes to provide formation of binaries like CuS, SnS, ZnS and then raised to 823.15 K, a temperature was maintained at 823.15 K for 30, 45 and 60 min to investigate the effect of sulfurization time on the properties of CZTS films. In our previous report, it was shown that the uniformity and density of the CZTS films increased for sulfurization temperatures between 823.15 K–843.15 K [40]. Therefore, sulfurization was performed at 823.15 K. After sulfurization, the films were cooled naturally (about 1 h). The final thickness of the CZTS films after sulfurization was around 1.2 μm. Growth parameters and structures of the samples discussed in this work are given in Table 1. Zn(O,S) buffer layers with a thickness of 50 nm were deposited on fabricated CZTS absorber layers by reactive RF magnetron sputtering from a ceramic ZnS target with 2-in. diameter. Typical deposition parameters were a base pressure of 0.26 mPa, an RF power of 40 W and target to substrate distance was 8 cm. During deposition, substrate temperature was fixed at 473.15 K to improve the crystalline quality and the adhesion of the films. Ar and O_2 gases were fixed at 50 sccm and 0.5 sccm, respectively, which resulted in Zn(O,S) layers with the S concentrations around X_s (S/S + O) = 0.53 with a band gap energy of 2.87 eV. The zinc oxide (ZnO) layers with a thickness of 40 nm were deposited on Zn(O,S) buffer layers by using a RF magnetron sputtering. Typical deposition parameters were a base pressure of 0.4 mPa, a working pressure of 1.12 Pa, an RF power of 50 W and target to substrate distance was 9 cm. Transparent conductive aluminum doped zinc oxide (AZO) layer was deposited onto ZnO layer by DC magnetron sputtering from 2-inch-ceramic targets of ZnO:Al_2O_3 ((98 wt% ZnO and 2 wt% Al_2O_3)) at room temperature [42]. Deposition was performed with an DC power of 50 W and 50 sccm Ar gas flow for 120 min. The AZO films have an average transmittance above 85% in the visible range (400–800 nm) and resistivity of 2.02×10^{-3} Ω.cm. After the deposition of AZO layer, the cell active area is defined out of a large area of the CZTS solar cell stack by removing the layers on top of the Mo outside the cell area. No anti-reflection coatings were deposited to cells. Finally, the cells were directly contacted with Ag epoxy via the window layer for electronic characterization.

To obtain information about crystal structures of the CZTS films, X-Ray Diffraction (XRD) was carried out in the Bragg-Brentano focusing geometry on a Phillips X'Pert Pro X-Ray diffractometry, with Cu Kα radiation (λ = 1.5406 Å). XRD patterns were recorded from 2θ = 20–80° with step size of 0.016° for all samples. A Veeco DEKTAK 150 profilometer was used to determine the thicknesses of the films. Raman studies were performed using High-resolution Raman spectroscopy (Princeton Instruments, Acton SP2750 0.750 mm Imaging Triple Grating Monochromator) in the back-scattering mode with spectral resolution of 1 cm^{-1} at room temperature. A wavelength of 488 nm and 514.5 nm Ion−Ar^+ was used with a 100 mW power. FEI-QuantaFEG 250 Scanning Electron Microscopy (SEM) with operating voltage of 20 kV was employed to characterize CZTS absorber and to have an idea about the morphology of the material, average grain size and the presence of undesired phases leaning on its surface. Energy Dispersive X-Ray Spectroscopy (EDS) analysis of the CZTS films was performed by FEI-QuantaFEG 250 SEM equipped with Oxford X-act EDS to determine the stoichiometry of the films. The performance of the CZTS thin film solar cell devices, such as Open circuit voltage (V_{oc}), Short circuit current density (J_{sc}), fill factor (FF) and η, was analyzed by current density-voltage (J-V) characterization. Keithley 2182A Source Meter and LabVIEW program were used to obtain J-V characteristics at room temperature. The calibration of our system was done using Newport 91,192 model 300 W solar simulator under ambient conditions (1 kW/m^2, AM 1.5G illumination, room temperature).

3. Results and discussion

3.1. Compositional and morphological analysis of CZTS thin films

SEM images of the Type 1 and Type 2 CZTS films sulfurized for different periods are shown in Fig. 1. For both Type 1 and Type 2 samples, there are no significant changes in the microstructure with respect to sulfurization time. SEM images of all samples indicate that CZTS films contains large grains with a size around 800 nm. For Type 1 CZTS thin films, sample A and B shows large flat crystals over the sample surface as can be seen in Fig. 1(a) and (b). According to our preliminary works on the morphology of the CZTS films, these crystals are attributed to SnS_2 (Fig. 2). The EDS of one of the CZTS film is given

Table 1
Growth parameters of the samples.

		Layer ordering	Cu thickness (nm)		Sulfurization temperature (K)	Sulfurization duration (min)
			Bottom	Top		
Type 1	Sample A	Cu/Sn/Zn/Cu	55	120	823.15	30
	Sample B	Cu/Sn/Zn/Cu	55	120	823.15	45
	Sample C	Cu/Sn/Zn/Cu	55	120	823.15	60
Type 2	Sample D	Cu/Sn/Zn/Cu	120	55	823.15	30
	Sample E	Cu/Sn/Zn/Cu	120	55	823.15	45
	Sample F	Cu/Sn/Zn/Cu	120	55	823.15	60

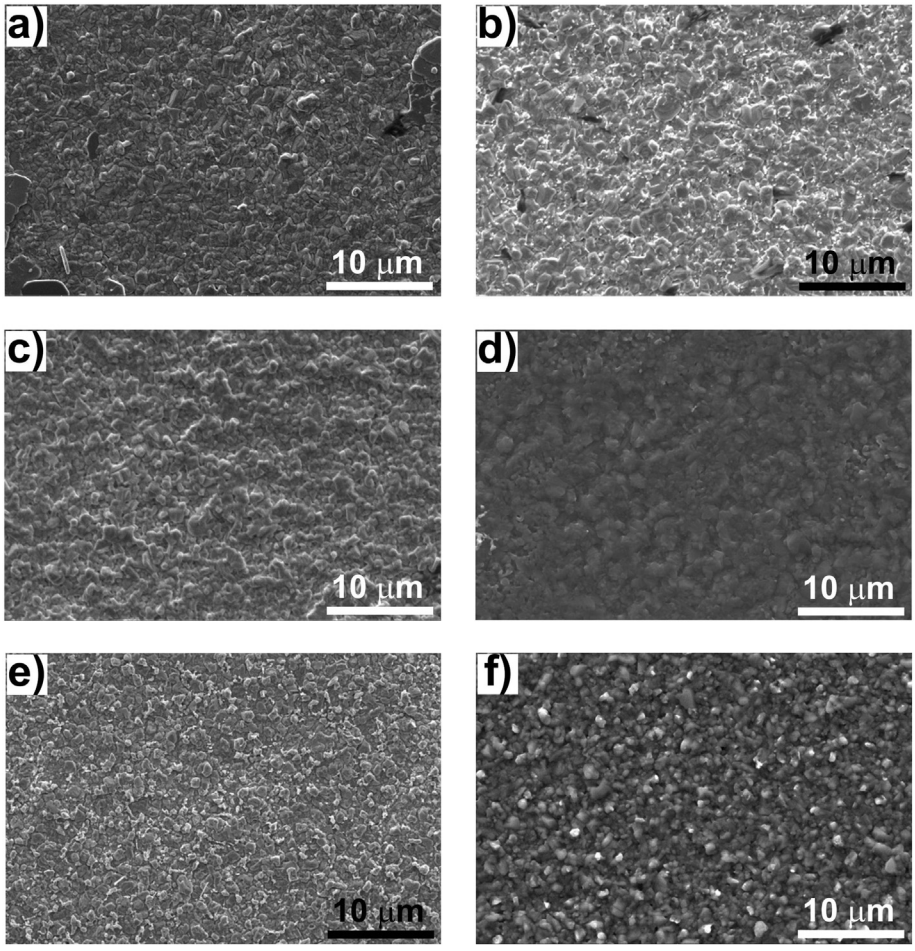

Fig. 1. SEM images of Type 1 and Type 2 CZTS samples a) Sample A b) Sample B, c) Sample C, d) Sample D e) Sample E and f) Sample F.

below. The crystals are mainly composed of Sn and S, detection of Cu and Zn is due to penetration of electrons through the sample. Our attribution is also consistent with the works on SnS_2 secondary phase in CZTS [43,44].

The formation of SnS_2 phase over the sample surface is evidence of leaving of Sn from the film. This instability of the Sn during the sulfurization of the CZTS limits the sulfurization time due to Sn losses. For short sulfurization duration, there are many SnS_2 crystals on the surface which indicates Sn-rich composition of the film. Increasing the sulfurization time leads to decrease in the amount of SnS_2 phase over the surface. Finally, it disappears for long sulfurization duration due to the decomposition reaction of SnS_2, $2SnS_2\ (s) \rightarrow 2SnS\ (g) + S_2\ (g)$.

EDS spectroscopy was performed to investigate the effect of sulfurization time on the chemical composition of the synthesized CZTS

Table 2
The average elemental compositions and elemental ratios of the Type 1 and Type 2 CZTS thin films.

		Cu (at. %)	Zn (at. %)	Sn (at. %)	S (at.%)	$\frac{Zn}{(Sn)}$	$\frac{Cu}{(Zn+Sn)}$	$\frac{Sn}{(Cu+Zn+Sn)}$
Type 1	Sample A	20	11	14	54	0.80	0.79	1.20
	Sample B	27	15	12	46	1.19	0.98	0.87
	Sample C	28	15	12	45	1.25	1.04	0.83
Type 2	Sample D	22	12	12	54	0.98	0.89	1.19
	Sample E	21	12	12	55	1.01	0.89	1.21
	Sample F	21	12	12	55	1.01	0.85	1.20

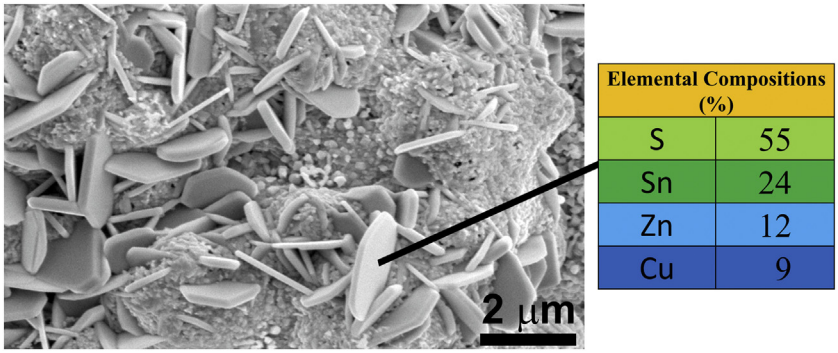

Fig. 2. SEM image and EDS result of SnS_2 crystals on CZTS.

thin films. Large area EDS scans were performed (approximately 150 μm^2) to include several grains. Table 2 shows the average elemental compositions and elemental ratios of the CZTS thin films. In fact, thicknesses of the Cu, Zn, and Sn films were adjusted to get Cu-poor and Zn-rich composition of the CZTS films by considering the molar fractions of Cu, Zn, and Sn. However, Different compositions were obtained due to the loss of Sn by the evaporation of SnS binary compound and evaporation of Zn.

For Type 1 samples, it is observed that Sn and S content decreases with increasing sulfurization time. For short sulfurization duration, high amount of SnS_2 phase over the surface results in S and Sn-rich composition of the film. When the sulfurization time increased, Sn composition of the film decreases due to Sn losses. By investigating the rates of Sn loss for the CZTS films and multilayers of binary sulfides, Weber et al. concluded that in addition to direct evaporation of SnS, there is a decomposition pathway of CZTS; Cu_2ZnSnS_4 (s) → Cu_2S (s) + ZnS (s) + SnS (g) + 1/2S_2 (g) [45]. According to the decomposition pathway of CZTS, SnS and disulfur (S_2) are assumed to evaporate from the surface of the sample. Both SnS_2 and CZTS decomposition reactions can explain why the amount of S reduces by decreasing amount of Sn in our samples.

For Type 2 samples, nearly same Sn and S content independent of sulfurization time have been observed. This behavior is attributed to higher Cu thickness at the bottom of precursor stack. To form CZTS, the last stage is through Cu_2SnS_3 + ZnS → Cu_2ZnSnS_4 [46,47]. During the sulfurization Cu and Sn react with S easily and Cu_2SnS_3 forms by the reaction of $Cu_{2-x}S$ with SnS_2. As discussed in the introduction part, when Cu is not adjacent to Sn, it's difficult to form Cu_2SnS_3 which is reactant to produce CZTS with ZnS [22,23,25]. It is thought that when Cu thickness at the bottom of the stack is high, more $Cu_{2-x}S$ and SnS_2 react and form Cu_2SnS_3 easily since higher amount of Cu adjacent to Sn. Since Sn is bounded by the formation of Cu_2SnS_3, Sn loss decreases. When Cu thickness at the bottom of the stack is low, less Sn is bounded, and Sn loss increases.

Fig. 3 shows how elemental ratios of the Type 1 and Type 2 samples change with sulfurization durations. While the relative ratios of Cu/(Zn + Sn), Zn/Sn, and S/(Cu + Zn + Sn) show different trends according to the sulfurization time due to formation of SnS_2 phases and the loss of Sn for Type 1 samples, these ratios show similar trend according to the sulfurization time for Type 2 samples. As mentioned previously, Cu-poor and Zn-rich composition, which is generally accepted in the literature for the realization of high efficiency CZTS devices, may be desirable to suppress the formation of Cu−S phases, harmful defects and defect clusters such as Cu_{Zn}, Cu_{Sn}, (Cu_{Sn} + Sn_{Cu}) and (Cu_{Zn} + Sn_{Zn}). However, due to volatility of Zn and Sn, both Cu-poor and Zn-rich composition for any of the samples could not be succeeded. While Cu-stochiometric and Zn-rich composition for Type 1 samples except for Sample A was obtained, Type 2 samples have Cu-poor and Zn-stochiometric composition. For Type 2 samples, Zn/Sn ratio close to 1 may eliminate the formation of ZnS phase which cause detrimental effect on CZTS devices. Cu-poor and Zn-poor composition with high S and Sn content for Sample A may indicate the higher amount of SnS_2 phase. For sample B and C, low S content below %50 with S/(Cu + Zn + Sn) < 1 was observed due to the loss of S resulting from decomposition reactions discussed above. It is believed that low S content in the CZTS films may cause the change of conduction from p-type to n-type and reduction of hole concentration due to high concentration of V_s [48]. For all Type 2 samples, S content above 50% with S/(Cu + Zn + Sn) > 1 was obtained which is important to reduce V_s and get higher p-type conductivity.

3.2. XRD analysis of CZTS thin films

CZTS compound may exist in two main crystal structures, known as kesterite (KS) and stannite (ST). Fig. 4 shows the XRD patterns of the CZTS films with Type 1 and Type 2 structure. It can be seen that all of the films have a polycrystalline structure and exhibit characteristics peaks of CZTS along (110), (112), (103), (200), (202), (211), (105), (220), (312), (224), (008) and (332) crystallographic directions at 2θ values 23.18, 28.53, 29.74, 33.04, 37.02, 37.96, 45.01, 47.40, 56.15, 58.93, 69.31 and 76.49°, respectively. Although XRD patterns match well with the standard XRD pattern of KS CZTS (JCPDS 26–0575) and those of the previously reported by other groups, peaks along (112), (200), (220), (312) and (224) directions at 2θ values 28.53, 33.04, 47.40, 56.15 and 58.93°, respectively, may indicate the presence of ZnS (JCPDS 05–0566) and Cu_2SnS_3 (JCPDS 027–0198) phases. It is clear from the XRD patterns that all the samples have good crystallinity and show preferential orientation along (112) direction with approximately same peak intensity. Extra peaks for Type 1 structure are attributed to the presence of tin dioxide (SnO_2) at 26.60° (110) and 33.85° (101), which are the preferential orientation for SnO_2 (JCPDS 041–1445). For Type 2 structure, extra peaks are attributed to the presence of ZnO (JCPDS 00–036-1451) at 34.50 (002) and 36.10° (101) and molybdenum dioxide (MoO_2) (JCPDS 00–032-0671) at 25.70° ($\bar{1}11$). Mo might be oxidized before placing the substrate into the magnetron sputtering system. Additional peaks at 42.58 couldn't be assigned any phases despite of detail investigation for Type 2 samples. A signal from the Mo back contact can be seen at 40.5° (110) (JCPDS 042–1120) for all samples. This peak also includes molybdenum disulfide (MoS_2) peak at 40.99° (JCPDS 024–0515). MoS_2 phase could not be distinguished by XRD since it has the strongest peak at 14.4° (JCPDS 024–0515) but this value is outside the measurement region of our XRD spectrometer. Moreover, the diffraction peaks at around 73.60° may correspond to both (205) diffraction peak of MoS_2 at 73.66° (JCPDS 037–1492) and

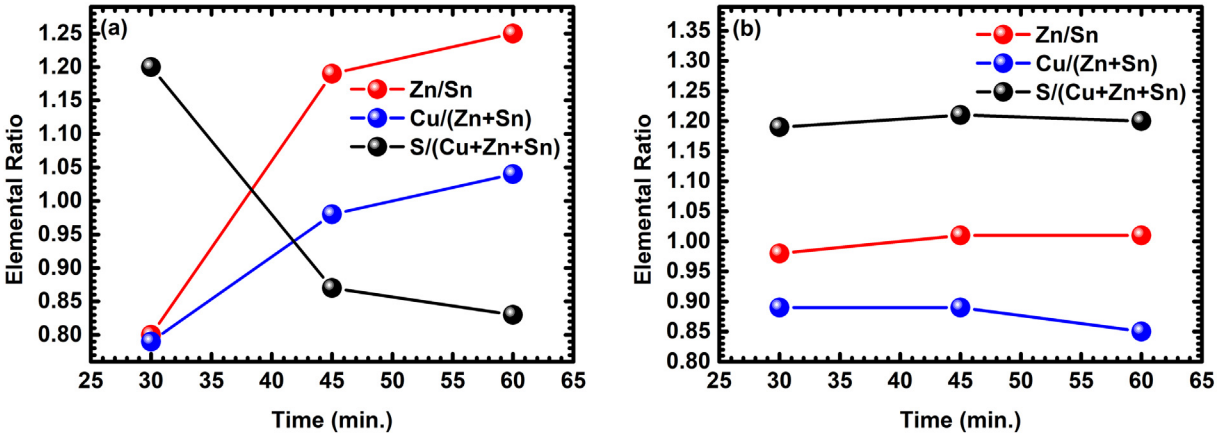

Fig. 3. Change in elemental ratios of the (a) Type 1 and (b) Type 2 CZTS samples with different sulfurization durations.

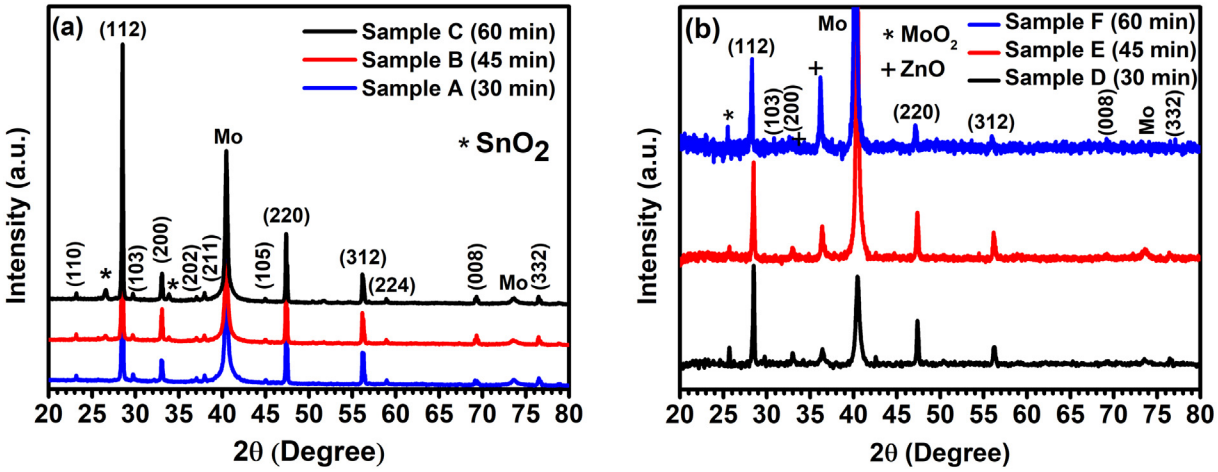

Fig. 4. XRD patterns of CZTS thin films with (a) Type 1 and (b) Type 2 structure.

(211) diffraction peak of Mo at 73.68° (JCPDS 042–1120). The peaks correspond to SnS_2 phase could not be detected by XRD (JCPDS 023–0677), it may be due to XRD detection limits or since this phase does not spread over the entire film surface. Moreover, SnS_2 has the strongest peak at 15.02° but this value was outside our measurement region.

ZnO, sulfur dioxide (SO_2) and SnO_2 are thermodynamically favorable native oxides on CZTS relative to copper oxide (CuO) since they have high enthalpy of formation [49]. However, SO_2 can easily evaporate due to its high vapor pressure. Evolution of SnO_2 interfacial phase over the sulfurization time can be clearly seen in the XRD graphs of CZTS films with Type 1 structure (Fig. 4(a)). While the films sulfurized for 30 min does not show any sign of SnO_2 phase, the films sulfurized for 45 min and 60 min show SnO_2 peaks along (200), and (332) crystallographic directions. Moreover, the intensity of the SnO_2 peak increases as the sulfurization time increases. These results indicate that sulfurization at high temperature (823.15 K) for longer durations trigger the formation of SnO_2 which results from oxygen exposure during the sulfurization. The formation of SnO_2 results from removing the Sn from the CZTS thin film and evidence of loss of Sn in CZTS. Moreover, considering the formation of SnO_2, it is thought that if the thick Cu layer is not adjacent to Sn layer, Cu cannot bound Sn by the formation of Cu_2SnS_3 and Sn loss increases. By considering SnO_2 as an indicator for Sn loss, it is concluded that the formation of SnO_2 cause the severe loss of Sn in CZTS and Sn loss increases for long sulfurization times due to more oxygen exposure. This tendency is in good agreement with the EDS results.

Evolution of ZnO interfacial phase over the sulfurization time can be clearly seen in the XRD graphs of CZTS films with Type 2 structure (Fig. 4(b)). The intensity of the ZnO peak increases as the sulfurization time increases which indicates that sulfurization for longer durations trigger the formation of ZnO at high temperature for the precursors having thin Cu cap layer. It is thought that this thin Cu cap layer cannot prevent the diffusion of Zn to the surface and formation of ZnO, while the formation of SnO_2 is prevented by thick Cu layer at the bottom of the stack.

3.3. Raman scattering analysis of CZTS thin films

The most probable ZnS cubic phase and both cubic and tetragonal Cu_2SnS_3 phases exhibit a crystal structure very similar to CZTS, so it is quite difficult to distinguish these phases from CZTS phase by XRD. Therefore, these absorbers have been further examined by the Raman spectroscopy. It is observed that the most intense peak in the Raman spectra of Type 1 samples lies between 330 and 332 cm^{-1} (Fig. 5(a)). In fact, A mode of KS has been observed between 331 and 338 cm^{-1} and varies with the synthesis method although reports of 337–338 cm^{-1} are the most common [50]. A mode results from vibrations of only anion lattice and its vibrational frequency w is given by $w = \sqrt{k/M_s}$, where k is the lattice vibration force constant and M_S is the atomic mass of S. In the case of Cu-poor and Zn-rich condition, respective bonds elongate by the expansion of the unit cell due to higher atomic weight of Zn (65.38 g/mol) than atomic weight of Cu (63.55 g/mol). Increase of the bond length tends to reduce the force constant and thus soften phonons mode to lower vibration frequency than A symmetry mode of KS at 338 cm^{-1}. Moreover, defects result from Cu-poor and Zn-rich condition such as Zn_{Cu} and V_{Cu} may promote additional non-center phonon scattering to the Raman line and results in Raman bandwidth broadening [51]. Shifting of the A mode of KS towards lower frequencies is attributed to the existence of disorder effects caused by the high concentration of intrinsic structural defects in the CZTS films. Even in stoichiometric compounds, the existence of Cu_{Zn} and Zn_{Cu} antisite defects has been demonstrated using neutron powder diffraction method [52]. It is now generally believed that CZTS crystallizes in the KS structure with the same amount of disordered KS phase. Presence of this disordered KS phase is characterized by a random distribution of Cu and Zn cations in the Cu—Zn planes and the leads to changes space symmetry from KS type I4 to a disordered KS phase I42m symmetry. The binding energy difference between KS and ST structures is about 3 meV/atom, thus, it may be supposed that the difference in binding energy between the KS and disordered KS structures may be < 3 meV/atom [53]. For Type 1 CZTS films, the formation of CZTS is confirmed by the presence of an intense peaks located at about 330 cm^{-1} which belongs to A mode of the disordered KS structure and weak peaks around 257 cm^{-1} (B(LO)) [54], and 270 cm^{-1} (A mode) [55]. Moreover, broad shoulders at the right and the left of the main CZTS peak can be explained by CZTS modes at 286 cm^{-1} (A mode), 308 cm^{-1} (B (TO) mode), and 370 cm^{-1} (B (LO) mode) [54–56]. These broad shoulders may possibly include peaks at 297 and 337 cm^{-1} for tetragonal Cu_2SnS_3, 303 cm^{-1} and 356 cm^{-1} for cubic Cu_2SnS_3, 318 cm^{-1} for orthorhombic Cu_2SnS_3, 275 and 352 cm^{-1} for cubic ZnS and 314 cm^{-1} for SnS_2 [57]. Peaks at 404 cm^{-1} corresponds to MoS_2 phase for Sample B and C [58]. Presence of this phase implies that part of CZTS absorber is not continuous which may lead to serious shunting. In addition, Raman measurements confirm the presence of SnO_2 phase by the broad peaks located around 475 cm^{-1} and 630 cm^{-1} [59].

Since Raman spectra of Type 1 samples give a general broadening due to the reduction in phonon correlation length caused by disorder, a special attention was given for the range 250–450 nm since main Raman modes of CZTS and many secondary phases lies in this range. In order to clarify the presence of the peaks was not experimentally resolved in our spectra, the experimental spectra were fitted with

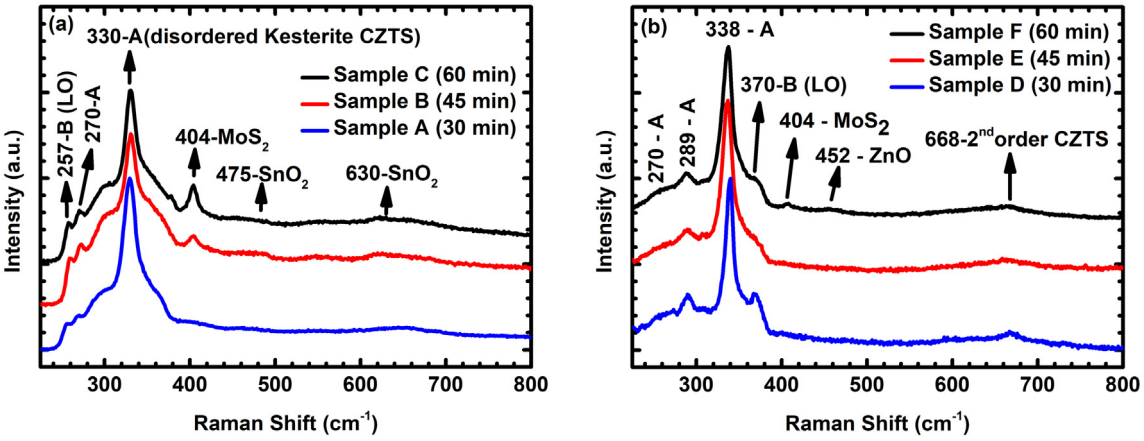

Fig. 5. Raman spectra of CZTS thin films with (a) Type 1 and (b) Type 2 structure.

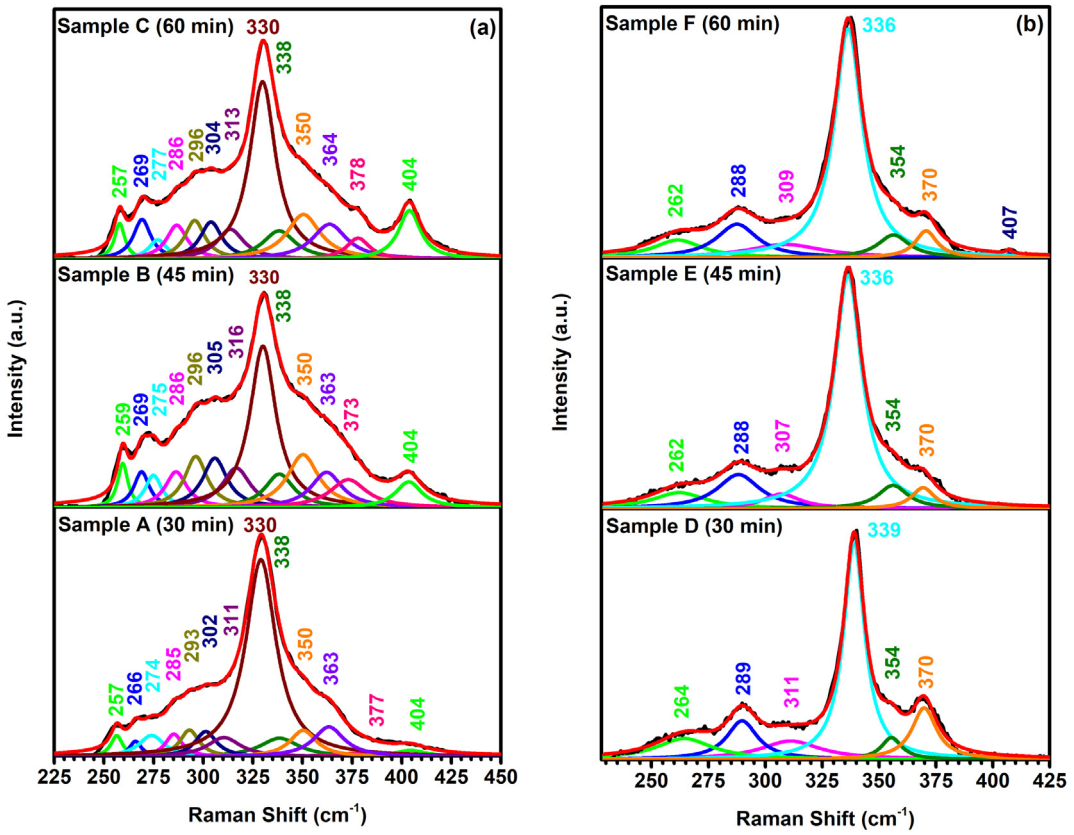

Fig. 6. Deconvoluted Raman spectra of CZTS thin films with (a) Type 1 and (b) Type 2 structure.

Lorentzian curves using Origin program (Fig. 6(a)). Firstly, it was assumed that the film contains only the KS CZTS structure, the peak positions were settled according to mostly reported Raman modes of KS CZTS with disordered KS peak at about 331 cm^{-1} and allowed to vary to get the best fit to the experimental spectra. Significant deviations were observed between the fixed peak positions before deconvolution and the varied peak positions after deconvolution. Then, presence of KS CZTS peak at about 338 cm^{-1} was taken into account and deconvolutions improved significantly. This indicates that both KS and disordered KS structures coexists in the real structure of our CZTS thin films with the dominance of disordered KS structure as can be seen in Fig. 6(a). To determine the goodness of fit, reduced chi-square and adjusted r square values were employed. During an iterative procedure, reduced chi-square value decreases and r-square value closes to 1 as the goodness of the fit increases. According to the deconvolution results, the main peak positions are around 330 cm^{-1} for the Type 1 films. In addition to the disordered KS peak, Type 1 films also have peaks at around 286 and 338 cm^{-1} which are assigned to the main vibrational A symmetry modes of KS CZTS [54–56]. Presence of these peaks point out that the Type 1 CZTS films are mixture of disordered KS and KS phases, which is not very unusual for non-stoichiometric compositions [60]. Type 1 films also show peaks at around 257 cm^{-1} and 268 cm^{-1} which are attributed to the B mode of longitudinal optical vibration (B(LO)) and A vibration modes of KS CZTS, respectively [55,56,61]. Peaks observed at around 275 cm^{-1} might be attributed to the ZnS secondary phase [57]. Peaks detected at 350 cm^{-1} may be attributed to both ZnS and B mode of transverse optical vibration (B(TO)) of KS CZTS [55,57]. Peaks around 313 cm^{-1} might be attributed to the SnS_2 secondary phase [57] or to B(TO) vibration of KS CZTS [55]. Peaks around 296 cm^{-1} and 304 cm^{-1} may be attributed to the tetragonal $Cu_2SnS_3$and Cubic

Cu_2SnS_3, respectively [57]. In addition, our deconvoluted spectrum give other contributions about 364 cm^{-1} and 377 cm^{-1} which are associated with the E(LO) mode and B(LO) mode of KS CZTS, respectively [54]. According to Raman analyses, presence of a ZnS and Cu_2SnS_3 phases cannot be ruled out for type 1 CZTS films. In fact, such broad shoulders at the right and the left of the main CZTS peak indicates the presence of Cu_2SnS_3 and ZnS phases even without deconvolution. Both disordered structure and remaining Cu_2SnS_3 and ZnS phases implies incomplete formation of CZTS.

In the Raman spectra of Type 2 samples, it is observed that the most intense peaks lie between 336 and 339 cm^{-1} (Fig. 5(b)) and they are attributed to A mode of KS with ordered structure. Weak peaks around 264, 289 and 370 cm^{-1} attributed to A, A and B (LO) modes, respectively [50,61]. For the sample F sulfurized for 60 min, extra peaks at around 407 cm^{-1} and at 452 cm^{-1} were observed. Peak at 407 cm^{-1} belongs to MoS_2 phase [58]. Peak at 452 cm^{-1} may be assigned to E_2 (High) mode of ZnO. However, direct attribution is not possible since this mode generally appears between 437 and 444 cm^{-1} [62]. In fact, due to the high optical band gaps of ZnS (~3.6 eV) and ZnO (~3.2 eV), 325 nm excitation wavelength would be needed for resonant Raman scattering analysis of pure ZnO [63] and ZnS [64]. MoO_2 observed in XRD analyses could not be detected due to the low penetration depth (170 nm) of laser. The broad band at 668 cm^{-1} can be attributed to second order of the main Raman band of CZTS [65]. Presence of this band indicates the improved crystalline quality of the material. As it can be seen from Fig. 5(b) and Fig. 6(b), almost all peaks can be directly detected in our experimental spectra. Peaks at 309 and 354 cm^{-1} were better resolved after deconvolution and may be attributed B(TO) vibration modes of KS CZTS. Peaks detected at 354 cm^{-1} may be also attributed to the ZnS secondary phase.

As it can be seen from Fig. 6(b), Raman curve shows less broadening in the range of 250–450 nm for Type 2 samples. Cubic ZnS is the only possible secondary phase may present in the CZTS films according to the deconvolution results [57]. For Type 2 samples, A mode of KS lies between 336 and 339 cm^{-1} with a narrower bandwidth which indicates Type 2 samples have reduced number of defects compared to Type 1 samples since shifting of the A mode of KS towards lower frequencies are attributed to the existence of defects. Higher number of defects, and remaining Cu_2SnS_3 and ZnS phases indicate that the last stage reaction to form CZTS is restricted for Type 1 samples [25]. It has been shown that there is a correlation between the full width half maximum (FWHM) of the main Raman peak of CZTS at 338 cm^{-1} and the degree of Cu−Zn ordering, the FWHM become smaller for more ordered materials [66]. Increase in the FWHM of the main Raman peak of CZTS indicates enhancement of disordering. Among all samples, it is thought that the Sample D has highest degree of ordering in CZTS because it has the highest frequency of main A mode and the narrowest bandwidth.

3.4. I−V characterization of CZTS solar cells

Fig. 7 show the dark J-V and light J-V curves of devices fabricated using Type 1 and Type 2 CZTS absorber layers, respectively. In order to prevent confusion, they are called as Type 1 and Type 2 devices according to their absorber layers. Minutes in the graphs represents the sulfurization times of the CZTS absorber layers. Dark J-V characteristics of all devices indicate the formation of high quality junction between the CZTS absorber and Zn(O,S) buffer. Strong distortion of the J-V curve under light can be seen, the curve shows a kink-like shape in the forward bias direction. CZTS solar cell devices fabricated in this work mainly suffer from low FF and J_{sc} essentially due to this distortion. J-V distortion, the reduced J_{sc} and the reduced FF can be explained by the barriers at the hetero-junctions [67]. The barrier height is defined as the distance between the Zn(O,S) conduction band at the Zn(O,S)/CZTS interface and the electron Fermi level (E_F) at the ZnO/Zn(O,S) interface. Spike like conformation between buffer and absorber layer forms a secondary barrier. If the barrier height is high, it may restrict electron transport and thus leads to the J-V distortion. The CBO between CZTS and Zn(O,S), electron doping density the Zn(O,S) and band gap of Zn(O,S) are the main factors that affect the barrier height [68].

As it seen from the light J-V curves, the photocurrent starts to become blocked at a reverse bias. The net current is small and equal to the photocurrent at 0 V. The small photocurrent indicates the high barrier height for the electrons. At higher voltages around 200 mV, there is also diode current and shunt current in addition to photocurrent. Therefore, the net current decreases from suddenly due to impeded photo-current collection. This leads to kinked J-V curve and significantly decreases the FF of the device. At higher voltages, J-V crossover occurs due to voltage dependence photocurrent for all devices. Under illumination, the net electric field, which separates the photo-generated carriers, vanishes at the built-in potential. Built-in potential depends on barrier height. Since the barrier is reduced due to the electron-hole pairs generated by the photons, built-in potential under illumination is lower than that of dark. As a result, dark and light J-V curves are crossover. The net photocurrent becomes zero at the built-in potential where crossover occurs since there is an equal probability for photo-generated carriers two diffuse to either of the two contacts. When the cell is biased to larger voltage, direction of the electric field and photocurrent change.

Strong dependence of device performances on both sulfurization time and the thickness of bottom Cu layer in CZTS precursors is further observed. As it can be seen, J_{sc}, V_{oc} and η values are reduced with increasing sulfurization time. Moreover, Type 2 CZTS cells, which have high thickness of bottom Cu layer in CZTS precursors, have higher performance parameters at a certain sulfurization time. Impeded photocurrent collection due to high barrier height has a negative effect on the device performance which results in reduced FF and J_{sc}. There are also many other factors that are critical for the performance of CZTS solar cells such as secondary phases in the bulk CZTS and ordering level of CZTS. Possible presence of ZnS and Cu_2SnS_3 phases realized by Raman analyses for CZTS films with Type 1 structure. The presence of ZnS can give insulator regions in the CZTS due to its the high band gap (3.6 eV). It does not influence the V_{oc} but can cause an increase in the series resistance because of its low conductivity. ZnS segregations can both reduce the active area and inhibit the current conduction in the absorber, reduces the device performance. Cu_2SnS_3, which is a p-type semiconductor with metallic character, can reduce the E_g and increase the conductivity of the device by forming a solid solution with CZTS. Both of minority and majority carriers flow to Cu_2SnS_3 due to its small E_g, thus it acts as a recombination center, reducing both J_{sc} and V_{oc}. SnS_2 observed in SEM analyses of Type 1 samples is a n-type semiconductor with a direct E_g of 2.2 eV. This secondary phase can act as an insulator, if it is present in larger quantities it is also possible to form a second diode with a polarity opposite to CZTS, which prevents the carrier collection and reduces the FF. SnO_2 and ZnO phases were observed in Type 1 and Type 2 CZTS films, respectively. Since these oxide phases have large bandgaps (E_g(ZnO) = 3.2 eV, E_g(SnO_2) = 3.8 eV), presence of these oxides may also give insulator regions in the CZTS and reduce the device performance. Moreover, high amount of these oxides leads to high densities of antisite disorder, thus causing reduction of V_{oc}.

An over-thick MoS_2 layer may also deteriorate the electrical contact. Side view SEM images of the Type 2 samples were given in Fig. 8 to show the formation and evolution of a MoS_2 interfacial layer over the sulfurization time. In these images, 1st Mo layer indicates the Mo layer produced at higher working pressure an 2nd Mo indicates the Mo layer produced at lower working pressure. Formation of MoS_2 can occur through decomposition reactions at CZTS/Mo and/or during the CZTS sulfurization process which supply S [69]. Since MoS_2 is indirect semiconductor with a low E_g of 1.29 eV, it reduces the V_{oc} of CZTS solar cells [70]. The thickness of the MoS_2 phase was determined as 59, 126 and 225 nm for sulfurization durations of 30, 45 and 60 min, respectively. This indicate that sulfurization for longer durations at high

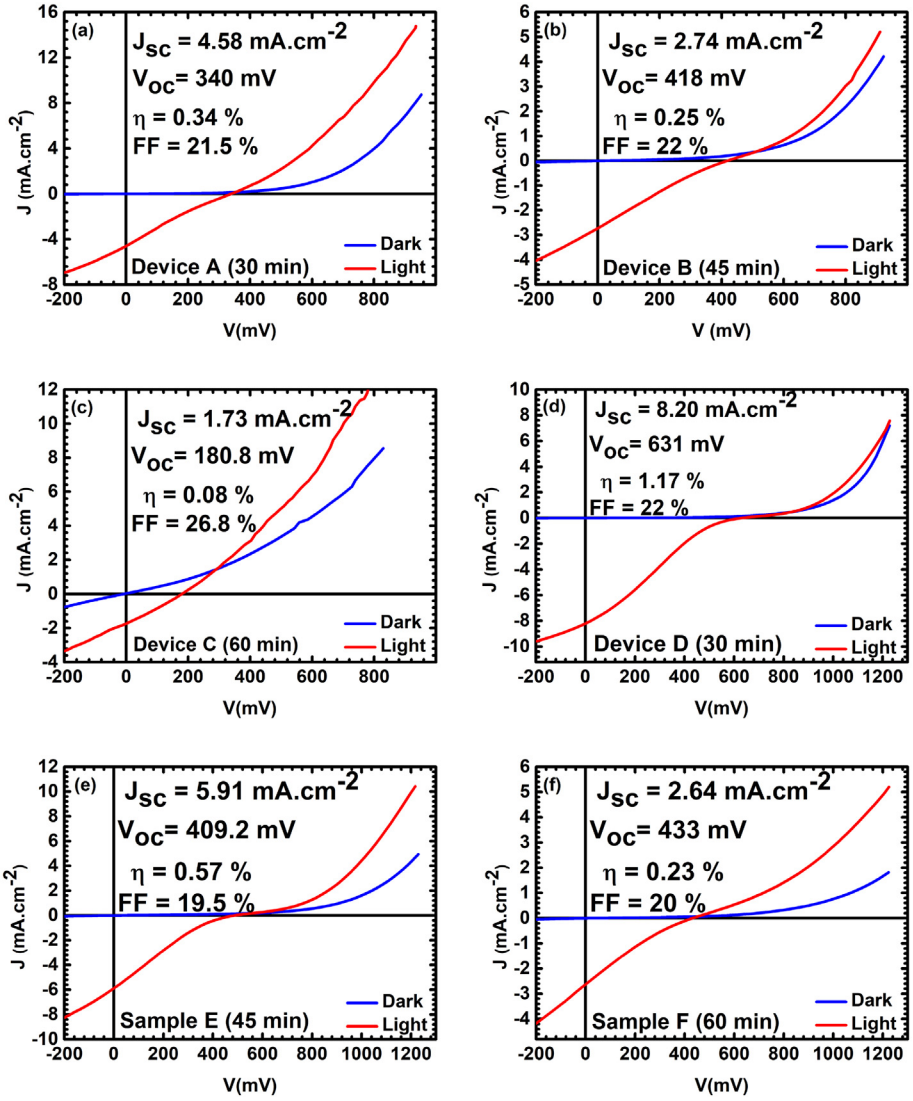

Fig. 7. J-V curves of Type 1 CZTS solar cells (a) Device A (b) Device B (c) Device C and Type 2 CZTS solar cells (d) Device D (e) Device E (f) Device F.

temperature trigger the formation of MoS_2. V_{oc} values of both Type 1 and Type 2 cells does not monotonically changed with the thickness of MoS_2 different than expected. Because, there are many other factors that affect V_{oc} [71,72]. Considering all these factors together, it is understandable that V_{oc} values do not change monotonically with Mo thickness.

Voids results from out-diffusion of elements and the decomposition of CZTS films have been observed near the CZTS/Mo interface. Reduced adhesion of CZTS on MoS_2 due to high amount of voids can be seen at high sulfurization duration. These voids may act as recombination centers, lower J_{sc} and V_{oc}. Moreover, they can act as shunting paths and decrease the shunt resistance [73]. These indicate that low sulfurization time is favorable to obtain MoS_2 layer with low thickness and restrict to void formation.

Due to Cu_{Zn} and Zn_{Cu} antisite defects, the change in the ordering level depending on thickness of Cu adjacent to Sn was observed in Raman spectroscopy analyses. Timmo, et al. have suggested that improved ordering increase the E_g of the CZTS and result in enhancement of V_{oc} [72]. It should be noted that the change in the band gap energy (ΔE_g) is followed by change in V_{oc} for an ideal solar cell. Additionally, high densities of antisite disorder (Cu_{Zn}, Zn_{Cu}) lead to band tailing, thus causing reduction of V_{oc} [74]. Improvement of V_{oc} due to increased Cu−Zn ordering has been also observed for $Cu_2ZnSnSe_4$ [75] and $Cu_2ZnSn(S,Se)_4$ [76]. According to these works, enhancement of V_{oc} for

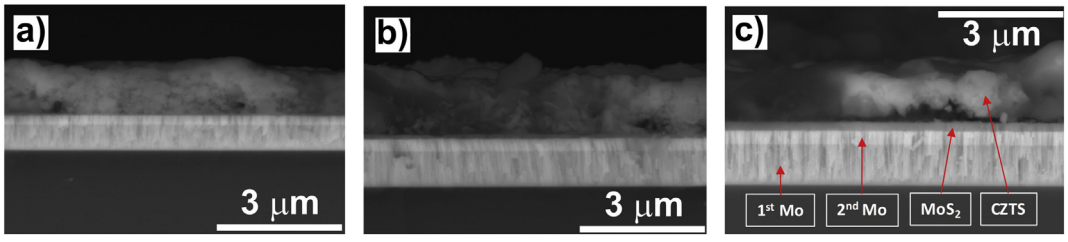

Fig. 8. Cross-section image of (a) Sample D (b) Sample E (c) Sample F showing evolution of MoS_2 at the Mo/CZTS interface.

Type 2 devices may be also attributed to the improved ordering of the samples. Among all samples, the highest degree of ordering in CZTS was obtained for Sample D which has also highest V_{oc}.

All phases present in CZTS absorbers explains how the thickness of the bottom Cu layer in CZTS precursors affect device performances. Higher degree of ordering and complete CZTS formation with less secondary phases for Type 2 absorber layers with thicker Cu layer adjacent to Sn layer in precursors provides better device performances. Among these phases, formation and evolution with increasing sulfurization time is only observed for the MoS_2, ZnO and SnO_2 phases. Therefore, degradation of the device performances with increasing sulfurization time is mainly attributed to formation and evolution of the MoS_2 and SnO_2 phases for Type 1 devices and MoS_2 and ZnO for Type 2 devices with increasing sulfurization time. Reduction of J_{sc} with increasing sulfurization time can be results from the evolution of the ZnO and SnO_2 phases. As in EDS, XRD and Raman analyzes, J-V results also confirms that Type 2 structure and 30 min sulfurization of CZTS precursors is the best to have better device performances. It should be specified that the devices fabricated from CZTS absorbers sulfurized at shorter durations (15 and 20 min) have not worked which may be due to incomplete formation of CZTS phase.

4. Conclusion

To develop relatively new, rapidly developing CZTS thin film solar cells, CZTS absorber layers were investigated to identify the impact of the growth conditions on film properties, optimize the growth process and apply the developed films to CZTS devices. CZTS films based on a stacked precursor (Cu/Sn/Zn/Cu) were prepared. The effect of sulfurization time and the thickness of top and bottom Cu layer in precursor on the properties of CZTS thin films were investigated. Based on SEM, EDS, XRD and Raman analyzes, it was concluded that 1) if the thick Cu layer is not adjacent to Sn layer, Sn loss increases, 2) when thick Cu layer is not adjacent to Sn, formation of CZTS is restricted, films exhibit disordered structure with many secondary phases, 3) thin Cu cap layer cannot prevent the Zn loss, while the Sn loss is prevented by thick Cu layer at the bottom of the stack, 4) the sulfurization time should be lowered to avoid the Sn an Zn losses and formation of the oxide phases. After the optimization of the growth process, CZTS solar cells were fabricated using only the magnetron sputtering technique for all thin films in the cell structure which provide easy adaptation to large-scale and reproducible manufacturing of the CZTS solar cells. As in CZTS thin film analyzes, J-V results also confirmed that thicker Cu layer should be adjacent to Sn layer in precursors and low sulfurization time of precursors are needed to have better device performances. The best device yielded a power conversion efficiency of 1.17% with a V_{oc} = 631.0 mV, J_{sc} = 8.20 mA/cm^2 and FF = 22.6%. Conventionally used CdS buffer layer also substituted with environmentally friendly alternative Zn(O,S) buffer layer in CZTS solar cells.

Acknowledgements

This research was supported in part by the TUBITAK (Scientific and Technical Research Council of Turkey) project number 114F341 and the authors would like to acknowledge the facilities of Applied Quantum Research Center (AQuReC) for the current study.

References

[1] M.A. Green, Y. Hishikawa, W. Warta, E.D. Dunlop, D.H. Levi, J. Hohl-Ebinger, A.W. Ho-Baillie, Solar cell efficiency tables (version 50), Prog. Photovolt. Res. Appl. 25 (2017) 668–676.
[2] P. Jackson, R. Wuerz, D. Hariskos, E. Lotter, W. Witte, M. Powalla, Effects of heavy alkali elements in Cu(In,Ga)Se_2 solar cells with efficiencies up to 22.6%, Phys. Status Solidi RRL 10 (8) (2016) 583–586.
[3] H. Katagiri, N. Ishigaki, T. Ishida, K. Saito, Characterization of Cu_2ZnSnS_4 thin films prepared by vapor phase sulfurization, Jpn. J. Appl. Phys. 40 (2R) (2001) 500.
[4] S. Yazici, M.A. Olgar, F.G. Akca, A. Cantas, M. Kurt, G. Aygun, E. Tarhan, E. Yanmaz, L. Ozyuzer, Growth of Cu_2ZnSnS_4 absorber layer on flexible metallic substrates for thin film solar cell applications, Thin Solid Films 589 (2015) 563–573.
[5] H. Katagiri, N. Sasaguchi, S. Hando, S. Hoshino, J. Ohashi, T. Yokota, Preparation and evaluation of Cu_2ZnSnS_4 thin films by sulfurization of E-B evaporated precursors, Sol. Energy Mater. Sol. Cells 49 (1–4) (1997) 407–414.
[6] H. Hiroi, N. Sakai, T. Kato, H. Sugimoto, High voltage Cu2ZnSnS4 submodules by hybrid buffer layer, Proc. of the 40th IEEE Photovoltaic Spec. Conf., Tampa FL, (2013), p. 863.
[7] S. Tajima, M. Umehara, M. Hasegawa, T. Mise, T. Itoh, Cu_2ZnSnS_4 photovoltaic cell with improved efficiency fabricated by high-temperature annealing after CdS buffer-layer deposition, Prog. Photovolt. Res. Appl. 25 (1) (2017) 14–22.
[8] D.B. Mitzi, O. Gunawan, T.K. Todorov, K. Wang, S. Guha, The path towards a high-performance solution-processed kesterite solar cell, Sol. Energy Mater. Sol. Cells 95 (2011) 1421–1436.
[9] I. Olekseyuk, I. Dudchak, L. Piskach, Phase equilibria in the Cu_2S-ZnS-SnS_2 system, J. Alloys Compd. 368 (1) (2004) 135–143.
[10] J.J. Scragg, Studies of Cu_2ZnSnS_4 films prepared by sulfurisation of electro-deposited precursors, Ph.D. Dissertation University of Bath, UK, 2010.
[11] A. Nagoya, R. Asahi, R. Wahl, G. Kresse, Defect formation and phase stability of Cu_2ZnSnS_4 photovoltaic material, Phys. Rev. B 81 (2010) 113202.
[12] A. Redinger, D.M. Berg, P.J. Dale, S. Siebentritt, The consequences of kesterite equilibria for efficient solar cells, J. Am. Chem. Soc. 133 (2011) 3320.
[13] S. Chen, J.-H. Yang, X.-G. Gong, A. Walsh, S.-H. Wei, Intrinsic point defects and complexes in the quaternary kesterite semiconductor Cu_2ZnSnS_4, Phys. Rev. B 81 (24) (2010) 245204.
[14] H. Katagiri, K. Jimbo, S. Yamada, T. Kamimura, W.S. Maw, T. Fukano, T. Ito, T. Motohiro, Enhanced conversion efficiencies of Cu_2ZnSnS_4-based thin film solar cells by using preferential etching technique, Appl. Phys. Express 1 (4) (2008) 041201.
[15] H. Katagiri, K. Jimbo, W.S. Maw, K. Oishi, M. Yamazaki, H. Araki, A. Takeuchi, Development of CZTS-based thin film solar cells, Thin Solid Films 517 (7) (2009) 2455–2460.
[16] S. Chen, A. Walsh, X.G. Gong, S.H. Wei, Classification of lattice defects in the kesterite Cu_2ZnSnS_4 and $Cu_2ZnSnSe_4$ earth-abundant solar cell absorbers, Adv. Mater. 25 (11) (2013) 1522–1539.
[17] B. Shin, O. Gunawan, Y. Zhu, N.A. Bojarczuk, S.J. Chey, S. Guha, Thin film solar cell with 8.4% power conversion efficiency using an earth-abundant Cu_2ZnSnS_4 absorber, Prog. Photovolt. Res. Appl. 21 (1) (2013) 72–76.
[18] T.K. Todorov, J. Tang, S. Bag, O. Gunawan, T. Gokmen, Y. Zhu, D.B. Mitzi, Beyond 11% efficiency: characteristics of state-of-the-art $Cu_2ZnSn(S,Se)_4$ solar cells, Adv. Energy Mater. 3 (1) (2013) 34–38.
[19] W. Wang, M.T. Winkler, O. Gunawan, T. Gokmen, T.K. Todorov, Y. Zhu, D.B. Mitzi, Device characteristics of CZTSSe thin-film solar cells with 12.6% efficiency, Adv. Energy Mater. 4 (7) (2014) 1301465.
[20] S. Marchionna, P. Garattini, A. Le Donne, M. Acciarri, S. Tombolato, S. Binetti, Cu_2ZnSnS_4 solar cells grown by sulphurisation of sputtered metal precursors, Thin Solid Films 542 (2013) 114–118.
[21] S.W. Shin, S.M. Pawar, C.Y. Park, J.H. Yun, J.-H. Moon, J.H. Kim, J.Y. Lee, Studies on Cu_2ZnSnS_4 (CZTS) absorber layer using different stacking orders in precursor thin films, Sol. Energy Mater. Sol. Cells 95 (2011) 3202–3206.
[22] H. Araki, A. Mikaduki, Y. Kubo, T. Sato, K. Jimbo, W.S. Maw, H. Katagiri, M. Yamazaki, K. Oishi, A. Takeuchi, Preparation of Cu_2ZnSnS_4 thin films by sulfurization of stacked metallic layers, Thin Solid Films 517 (2008) 1457–1460.
[23] H. Yoo, J.H. Kim, Growth of Cu_2ZnSnS_4 thin films using sulfurization of stacked metallic films, Thin Solid Films 518 (22) (2010) 6567–6572.
[24] P.A. Fernandes, P.M.P. Salomé, A.F. Da Cunha, Precursors' order effect on the properties of sulfurized Cu_2ZnSnS_4 thin films, Semicond. Sci. Technol. 24 (10) (2009) 105013.
[25] C.Y. Su, C.Y. Chiu, J.M. Ting, Cu_2ZnSnS_4 absorption layers with controlled phase purity, Sci. Rep. 5 (2015) 9291.
[26] L. Weinhardt, O. Fuchs, D. Groß, G. Storch, E. Umbach, N.G. Dhere, A.A. Kadam, S.S. Kulkarni, C. Heske, Band alignment at the CdS/Cu(in,Ga)S_2 interface in thin-film solar cells, Appl. Phys. Lett. 86 (6) (2005) 062109.
[27] M. Buffière, S. Harel, C. Guillot-Deudon, L. Arzel, N. Barreau, J. Kessler, Effect of the chemical composition of co-sputtered Zn(O, S) buffer layers on Cu(in, Ga)Se_2 solar cell performance, Phys. Status Solidi A 212 (2) (2015) 282–290.
[28] S.K. Pandey, S. Pandey, V. Parashar, R.S. Yadav, G. Mehrotra, A.C. Pandey, Bandgap engineering of colloidal zinc oxysulfide via lattice substitution with sulfur, Nanoscale 6 (3) (2014) 1602–1606.
[29] C. Platzer-Björkman, J. Lu, J. Kessler, L. Stolt, Interface study of CuInSe_2/ZnO and Cu(in, Ga)Se_2/ZnO devices using ALD ZnO buffer layers, Thin Solid Films 431 (2003) 321–325.
[30] P. Sinsermsuksakul, K. Hartman, S.B. Kim, J. Heo, L. Sun, H.H. Park, R. Chakraborty, T. Buonassisi, R.G. Gordon, Enhancing the efficiency of SnS solar cells via band-offset engineering with a zinc oxysulfide buffer layer, Appl. Phys. Lett. 102 (5) (2013) 053901.
[31] L. Sun, R. Haight, P. Sinsermsuksakul, S. Bok Kim, H.H. Park, R.G. Gordon, Band alignment of SnS/Zn(O, S) heterojunctions in SnS thin film solar cells, Appl. Phys. Lett. 103 (18) (2013) 181904.
[32] C. Platzer-Björkman, T. Törndahl, D. Abou-Ras, J. Malmström, J. Kessler, L. Stolt, Zn(O, S) buffer layers by atomic layer deposition in Cu(In, Ga)Se_2 based thin film solar cells: band alignment and sulfur gradient, J. Appl. Phys. 100 (4) (2006) 044506.
[33] Solar Frontier, Solar Frontier sets thin-film PV world record with 20.9% CIS cell,

http://www.solar-frontier.com/eng/news/2014/C031367.html/, (2014) (accessed 04 November 2018).
[34] T.M. Friedlmeier, P. Jackson, A. Bauer, D. Hariskos, O. Kiowski, R. Wuerz, M. Powalla, Improved photocurrent in Cu(In, Ga)Se_2 solar cells: from 20.8% to 21.7% efficiency with CdS buffer and 21.0% Cd-free, IEEE J. Photovoltaics 5 (5) (2015) 1487–1491.
[35] R. Klenk, A. Steigert, T. Rissom, D. Greiner, C.A. Kaufmann, T. Unold, M.C. Lux-Steiner, Junction formation by Zn(O, S) sputtering yields CIGSe-based cells with efficiencies exceeding 18%, Prog. Photovolt. Res. Appl. 22 (2) (2014) 161–165.
[36] T. Ericson, J.J. Scragg, A. Hultqvist, J.T. Watjen, P. Szaniawski, T. Torndahl, C. Platzer-Bjorkman, Zn(O, S) Buffer Layers and Thickness Variations of CdS Buffer for Cu_2ZnSnS_4 Solar Cells, IEEE J. Photovoltaics 4 (1) (2014) 465–469.
[37] C. Yan, F. Liu, N. Song, Boon K. Ng, J.A. Stride, A. Tadich, X. Hao, Band alignments of different buffer layers (CdS, Zn(O, S), and In_2S_3) on Cu_2ZnSnS_4, Appl. Phys. Lett. 104 (17) (2014) 173901.
[38] S. Karthikeyan, L. Zhang, S.A. Campbell, In-situ stress and thermal stability studies of molybdenum bilayer back contacts for photovoltaic applications, Proc. of the 40th IEEE Photovoltaic Spec. Conf., Denver CO, 2014, p. 387.
[39] H. Scofield, A. Duda, D. Albin, B. Ballard, P. Predecki, Sputtered molybdenum bi-layer back contact for copper indium diselenide-based polycrystalline thin-film solar cells, Thin Solid Films 260 (1) (1995) 26–31.
[40] D. G. Buldu, A. Cantas, F. Turkoglu, G. Akca, E. Meric, M. Ozdemir, E. Tarhan, L. Ozyuzer, G. Aygun, Influence of sulfurization temperature on Cu_2ZnSnS_4 absorber layer on flexible titanium substrates for thin film solar cells, Phys. Scr. 93 (2017) 024002.
[41] K. Wang, O. Gunawan, T. Todorov, B. Shin, S. Chey, N. Bojarczuk, D. Mitzi, S. Guha, Thermally evaporated Cu_2ZnSnS_4 solar cells, Appl. Phys. Lett. 97 (14) (2010) 143508.
[42] F. Turkoglu, H. Koseoglu, S. Zeybek, M. Ozdemir, G. Aygun, L. Ozyuzer, Effect of substrate rotation speed and off-center deposition on the structural, optical, and electrical properties of AZO thin films fabricated by DC magnetron sputtering, J. Appl. Phys. 123 (16) (2018) 165104.
[43] J.G. Bolke, Investigation of surface phase formation during, M. Sc. Dissertation The University of Utah, USA, 2012.
[44] W.H. Wang, G.L. Chen, H.L. Cai, B.W. Chen, L.Q. Yao, M. Yang, S.Y. Chen, Z.G. Huang, The effects of SnS_2 secondary phases on Cu_2ZnSnS_4 solar cells: a promising mechanical exfoliation method for its removal, J. Mater. Chem. A 6 (2018) 2995–3004.
[45] A. Weber, R. Mainz, T. Unold, S. Schorr, H.W. Schock, In-situ XRD on formation reactions of Cu_2ZnSnS_4 thin films, Phys. Status Solidi (c) 6 (5) (2009) 1245–1248.
[46] F. Hergert, R. Hock, Predicted formation reactions for the solid-state syntheses of the semiconductor materials Cu_2SnX_3 and Cu_2ZnSnX_4 (X = S, Se) starting from binary chalcogenides, Thin Solid Films 515 (15) (2007) 5953–5956.
[47] S. Schorr, A. Weber, V. Honkimäki, H.-W. Schock, In-situ investigation of the kesterite formation from binary and ternary sulphides, Thin Solid Films 517 (7) (2009) 2461–2464.
[48] M.-Y. Yeh, P.-H. Lei, S.-H. Lin, C.-D. Yang, Copper-Zinc-Tin-Sulfur Thin Film using Spin-Coating Technology, Materials 9 (7) (2016) 526.
[49] K. Sardashti, R. Haight, T. Gokmen, W. Wang, L.Y. Chang, D.B. Mitzi, A.C. Kummel, Impact of Nanoscale Elemental distribution in High-Performance Kesterite Solar Cells, Adv. Energy Mater. 5 (10) (2015) 1402180.
[50] A. Khare, B. Himmetoglu, M. Johnson, D.J. Norris, M. Cococcioni, E.S. Aydil, Calculation of the lattice dynamics and Raman spectra of copper zinc tin chalcogenides and comparison to experiments, J. Appl. Phys. 111 (8) (2012) 083707.
[51] E. Rudigier, I. Luck, R. Scheer, Quality assessment of $CuInS_2$-based solar cells by Raman scattering, Appl. Phys. Lett. 82 (24) (2003) 4370–4372.
[52] S. Schorr, H.J. Hoebler, M. Tovar, A neutron diffraction study of the stannite-kesterite solid solution series, Eur. J. Mineral. 19 (1) (2007) 65–73.
[53] M.Y. Valakh, O. Kolomys, S. Ponomaryov, V. Yukhymchuk, I. Babichuk, V. Izquierdo-Roca, E. Saucedo, A. Perez-Rodriguez, J.R. Morante, I.V. Bodnar, S. Schorr, Raman scattering and disorder effect in Cu_2ZnSnS_4, Phys. Status Solidi RRL 7 (4) (2013) 258–261.
[54] M. Dimitrievska, A. Fairbrother, X. Fontané, T. Jawhari, V. Izquierdo-Roca, E. Saucedo, A. Pérez-Rodríguez, Multiwavelength excitation Raman scattering study of polycrystalline kesterite Cu_2ZnSnS_4 thin films, Appl. Phys. Lett. 104 (2) (2014) 021901.
[55] M. Guc, S. Levcenko, I.V. Bodnar, V. Izquierdo-Roca, X. Fontane, L.V. Volkova, E. Arushanov, A. Pérez-Rodríguez, Polarized Raman scattering study of kesterite type Cu_2ZnSnS_4 single crystals, Sci. Rep. 6 (2016) 19414.
[56] D. Dumcenco, Y.S. Huang, The vibrational properties study of kesterite Cu_2ZnSnS_4 single crystals by using polarization dependent Raman spectroscopy, Opt. Mater. 35 (3) (2013) 419–425.
[57] P. Fernandes, P. Salomé, A. Da Cunha, Study of polycrystalline Cu_2ZnSnS_4 films by Raman scattering, J. Alloys Compd. 509 (28) (2011) 7600–7606.
[58] S.J. Sandoval, D. Yang, R.F. Frindt, J.C. Irwin, Raman study and lattice dynamics of single molecular layers of MoS_2, Phys. Rev. B 44 (8) (1991) 3955.
[59] Y.M. Lu, J. Jiang, M. Becker, B. Kramm, L. Chen, A. Polity, Y.B. He, P.J. Klara, B.K. Meyer, Polycrystalline SnO_2 films grown by chemical vapor deposition on quartz glass, Vacuum 122 ((2015) 347–352.
[60] A. Cantas, F. Turkoglu, E. Meric, F.G. Akca, M. Ozdemir, E. Tarhan, L. Ozyuzer, G. Aygun, Importance of CdS Buffer Layer Thickness on Cu_2ZnSnS_4 based Solar Cell Efficiency, J. Phys. D. Appl. Phys. 51 (2018) 275501.
[61] A. Khare, B. Himmetoglu, M. Cococcioni, E.S. Aydil, First principles calculation of the electronic properties and lattice dynamics of $Cu_2ZnSn(S_{1-x}Se_x)_4$, J. Appl. Phys. 111 (12) (2012) 123704.
[62] V. Russo, M. Ghidelli, P. Gondoni, C. Casari, A. Li Bassi, Multi-wavelength Raman scattering of nanostructured Al-doped zinc oxide, J. Appl. Phys. 115 (7) (2014) 073508.
[63] C. Insignares-Cuello, X. Fontané, Y. Sánchez-González, M. Placidi, C. Broussillou, J. López-García, E. Saucedo, V. Bermúdez, A. Pérez-Rodríguez, V. Izquierdo-Roca, Non-destructive assessment of ZnO: Al window layers in advanced Cu(in, Ga)Se_2 photovoltaic technologies, Phys. Status Solidi A 212 (1) (2015) 56–60.
[64] A. Fairbrother, L. Fourdrinier, X. Fontané, V. Izquierdo-Roca, M. Dimitrievska, A. Pérez-Rodríguez, E. Saucedo, Precursor Stack Ordering Effects in $Cu_2ZnSnSe_4$ Thin Films prepared by Rapid thermal Processing, J. Phys. Chem. C 118 (31) (2014) 17291–17298.
[65] M. Pal, N. Mathews, R.S. Gonzalez, X. Mathew, Synthesis of Cu_2ZnSnS_4 nanocrystals by solvothermal method, Thin Solid Films 535 (2013) 78–82.
[66] J.J. Scragg, L. Choubrac, A. Lafond, T. Ericson, C. Platzer-Björkman, A low-temperature order-disorder transition in Cu_2ZnSnS_4 thin films, Appl. Phys. Lett. 104 (4) (2014) 041911.
[67] A. Pudov, A. Kanevce, H. Al-Thani, J. Sites, F. Hasoon, Secondary barriers in CdS-$CuIn_{1-x}Ga_xSe_2$ solar cells, J. Appl. Phys. 97 (6) (2005) 064901.
[68] T. Song, Distortions to current-voltage curves of cigs cells with sputtered Zn(O, S) buffer layers, Ph.D. Dissertation Colorado State University, US, 2013.
[69] J.J. Scragg, T. Kubart, J.T. Wätjen, T. Ericson, M.K. Linnarsson, C. Platzer-Björkman, Effects of back contact instability on Cu_2ZnSnS_4 devices and processes, Chemistry of Materials 25 (15) (2013) 3162–3171.
[70] B. Shin, Y. Zhu, N.A. Bojarczuk, S. Jay Chey, S. Guha, Control of an interfacial $MoSe_2$ layer in $Cu_2ZnSnSe_4$ thin film solar cells: 8.9% power conversion efficiency with a TiN diffusion barrier, Appl. Phys. Lett. 101 (5) (2012) 053903.
[71] S. Tajima, T. Itoh, H. Hazama, K. Ohishi, R. Asahi, Improvement of the open-circuit voltage of Cu_2ZnSnS_4 solar cells using a two-layer structure, Appl. Phys. Express 8 (8) (2015) 082302.
[72] K. Timmo, M. Kauk-Kuusik, M. Pilvet, T. Raadik, M. Altosaar, M. Danilson, M. Grossberg, J. Raudoja, K. Ernits, Influence of order-disorder in Cu_2ZnSnS_4 powders on the performance of monograin layer solar cells, Thin Solid Films 633 (2016) 122–126.
[73] X. Liu, H. Cui, C. Kong, X. Hao, Y. Huang, F. Liu, N. Song, G. Conibeer, M. Green, Rapid thermal annealed Molybdenum back contact for Cu_2ZnSnS_4 thin film solar cells, Appl. Phys. Lett. 106 (13) (2015) 131110.
[74] T. Gokmen, O. Gunawan, T.K. Todorov, D.B. Mitzi, Band tailing and efficiency limitation in kesterite solar cells, Appl. Phys. Lett. 103 (10) (2013) 103506.
[75] G. Rey, T. Weiss, J. Sendler, A. Finger, C. Spindler, F. Werner, M. Melchiorre, M. Hála, M. Guennou, S. Siebentritt, Ordering kesterite improves solar cells: a low temperature post-deposition annealing study, Sol. Energy Mater. Sol. Cells 151 (2016) 131–138.
[76] C. Krämmer, C. Huber, T. Schnabel, C. Zimmermann, M. Lang, E. Ahlswede, H. Kalt, M. Hetterich, Order-disorder related band gap changes in $Cu_2ZnSn(S, Se)_4$: impact on solar cell performance, Proc. 42nd IEEE Photovoltaic Specialist Conference (PVSC), 2015.